JACS
JOURNAL OF THE AMERICAN CHEMICAL SOCIETY
pubs.acs.org/JACS
Article

Real-Time Direct Monitoring of Chirality Fixation and Recognition at the Single-Molecule Level

Weilin Hu,[⊥] Mingyao Li,[⊥] Wan Xiong,[⊥] Shuyao Zhou, Qi Zou,* Jing-Tao Lü,* He Tian, and Xuefeng Guo*

Cite This: J. Am. Chem. Soc. 2024, 146, 17765−17772
Read Online
ACCESS | Metrics & More | Article Recommendations | Supporting Information

ABSTRACT: Chirality, a fundamental attribute of nature, significantly influences a wide range of phenomena related to physical properties, chemical reactions, biological pharmacology, and so on. As a pivotal aspect of chirality research, chirality recognition contributes to the synthesis of complex chiral products from simple chiral compounds and exhibits intricate interplay between chiral materials. However, macroscopic detection technologies cannot unveil the dynamic process and intrinsic mechanisms of single-molecule chirality recognition. Herein, we present a single-molecule detection platform based on graphene-molecule-graphene single-molecule junctions to measure the chirality recognition involving interactions between amines and chiral alcohols. This approach leads to the realization of in situ and real-time direct observation of chirality recognition at the single-molecule level, demonstrating that chiral alcohols exhibit compelling potential to induce the formation of the corresponding chiral configuration of molecules. The amalgamation of theoretical analyses with experimental findings reveals a synergistic action between electrostatic interactions and steric hindrance effects in the chirality recognition process, thus substantiating the microscopic mechanism governing the chiral structure−activity relationship. These studies open up a pathway for exploring novel chiral phenomena from the fundamental limits of chemistry, such as chiral origin and chiral amplification, and offer important insights into the precise synthesis of chiral materials.

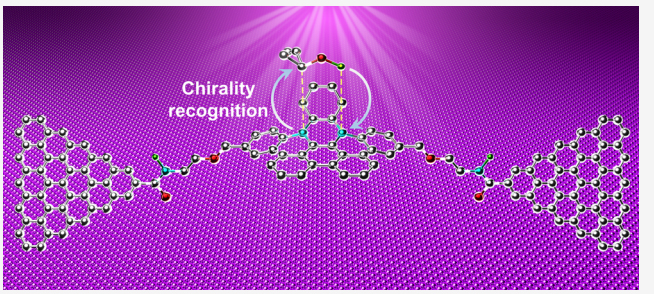

INTRODUCTION

Chirality has garnered substantial attention owing to its intrinsic properties[1] and special reactions.[2−6] In pursuit of introducing chirality into chemical reactions, several strategies have been proposed: (i) introduction of chiral substrates[7,8] and asymmetric catalysts;[9−12] (ii) introduction of the external chiral electromagnetic field;[13,14] and (iii) introduction of chiral auxiliaries,[15] which refer to chiral molecules that are temporarily added to control the stereochemical results of synthesis.[16,17] The introduction of a chiral auxiliary is a powerful method for transferring chirality from pre-existing chiral molecules to target molecules. The process often occurs along with chirality recognition in the presence of specific ionic pairs, hydrogen bonding pairs, metal coordination pairs, or covalent bondings.[18] However, the monitoring of the chirality process is often limited to macroscopic tests such as circular dichroism (CD) spectroscopy,[19] and the internal mechanisms of this process are difficult to observe owing to the ensemble-averaging effect. Because the single-molecule detection platform can considerably exclude the effects of ensemble averaging, it is possible to clarify the microscopic underlying mechanisms of the chirality recognition process by observing the full details at the single-molecule level.

In this study, in situ and real-time observations of chirality recognition were achieved using a single-molecule platform based on graphene-molecule graphene single-molecule junctions (GMG-SMJs). Both theoretical analysis and experimental evidence have consistently proved the synergistic action between the dipole interaction and the steric hindrance effect in chirality recognition. This synergy promotes strong interactions between molecules of identical chirality involving chiral alcohols and chiral tertiary amines at the single-molecule level, which further modulates the chirality recognition process. This work visualizes the detailed molecular-level process of chirality fixation and recognition, which aids in designing efficient chiral catalysts and novel nanomaterials as well as elucidating the origin of chirality.

Received: March 2, 2024
Revised: June 13, 2024
Accepted: June 14, 2024
Published: June 21, 2024

https://doi.org/10.1021/jacs.4c03071
J. Am. Chem. Soc. 2024, 146, 17765−17772

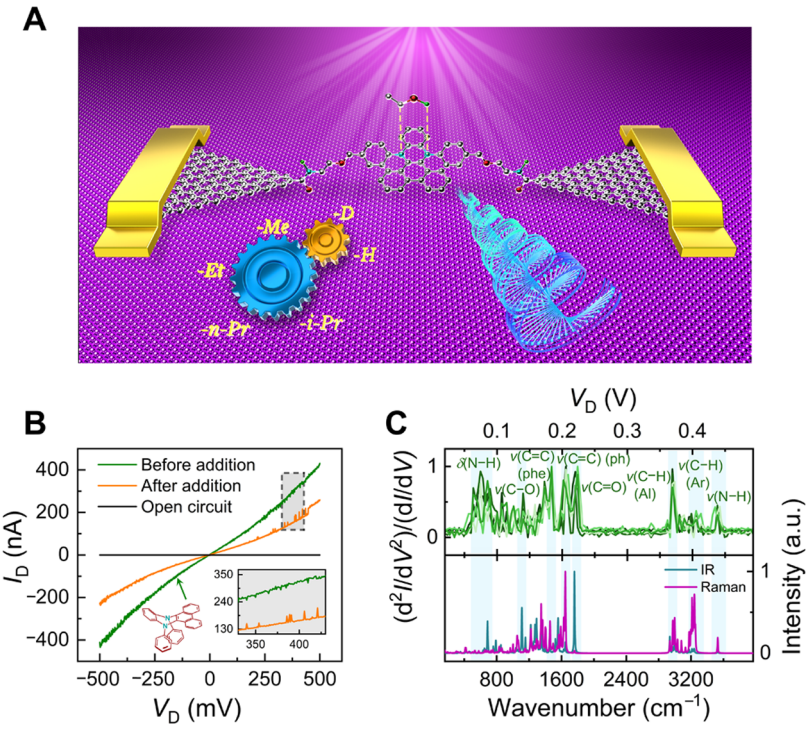

Figure 1. Structure and characterization of single-molecule devices. (A) Schematic diagram of an HON-based single-molecule device with ethanol adducted. The insets show different experimental conditions (alcohol type, deuterated conditions, and polarized light). (B) Electrical properties of a single-molecule device rejoined by HON at 300 K, showing the current−voltage (I−V) curves before (black) and after reconnection (green and orange colors represent HON before and after alcohol addition, respectively). The insets denote the structure of HON and an enlarged I−V curve. (C) Reproducible IETSs for the same HON-based single-molecule device measured five times at 2 K. The lock-in second-harmonic technique is adopted at an alternative current amplitude of 10.6 mV and a frequency of 661 Hz. The infrared and Raman spectra of HON (including the amide bonds) are calculated as well. The peaks assigned to specific vibrational modes are marked in the IETSs ($V = h\omega/e$). The peaks of δ(N−H) (~75 mV), ν(C−O) (~140 mV), ν(C═C) (phenanthrene) (~184 mV), ν(C═C) (benzene) (~202 mV), ν(C−H)(Al) (~369 mV) (for − CH_2 and − CH_3), and ν(C−H)(Ar) (~405 mV) (for −CH_2 and −CH_3) should be assigned to the molecular bridge. The peaks of ν(C═O) at ~224 mV and ν(N−H) at ~438 mV should be ascribed to the amide bond, respectively.

RESULTS AND DISCUSSION

Preparation and Characterization of HON-based GMG-SMJs. To elucidate the intricate process of single-molecule chirality recognition, a target system composed of chiral tertiary amines and chiral alcohols was chosen. The inherent flexibility characteristic of chiral flipping within tertiary amines facilitates the chirality recognition process. First, a verification process was conducted to confirm the molecular-level interaction between alcohols and tertiary amines based on a phenomenon termed "chirality fixation". To facilitate this investigation, a single-molecule device (Figure 1A) was fabricated via a methodology outlined in a previous protocol.[20,21] Briefly, graphene, which was grown by using chemical vapor deposition, was transferred to a silicon wafer, and it was then used to obtain a graphene-based field-effect transistor via continuous lithography and thermal evaporation. The dihydrodibenzo[a,c]phenazine-based molecule (abbreviated as HON) is a unique tertiary amine molecule with amino terminations, which was designed and synthesized for this study (inset of Figure 1B and Scheme S1).[22−24] The tertiary amine HON was effectively linked to the prepared graphene electrode through an amide reaction. Comprehensive details of molecular synthesis (Schemes S1 and S2 and Figures S39−S51) and the fabrication of the single-molecule device (Figures S1 and S2) can be found in the Supporting Information. To gauge the success of this connection between HON and graphene electrodes as well as the consequent formation of a closed-loop structure, a comprehensive assessment of the electrical properties, particularly the current−voltage (I−V) characteristics of the device at different stages, was conducted. The results (Figures 1B and S3) indicated the establishment of a closed-loop structure. The results of the binomial distribution analysis (Chapter 5 of the Supporting Information) showed that approximately 35% of these devices exhibited successful reconnections, and the proportion of single-molecule-connecting devices to the overall reconnected devices was ~83%. To provide further validation for the successful single-molecule connection, an optical demonstration[25] (Figure S4) and inelastic electron tunneling spectroscopies (IETSs) (Figure 1C) were conducted on HON-rejoined single-molecule devices. The results of these tests again confirmed the formation of a single-molecule connection.

Real-Time Measurement Before Chirality Fixation. A comprehensive investigation involving temperature-dependent and bias voltage-dependent tests was conducted on HON-based single-molecule devices (Figures S6−S11). The testing results indicated dominant transitions between the two electrical conductance states. With an increase in both the temperature and bias voltage, the frequency of these transitions increased. To specify the origin of these conductance states, a control molecule devoid of the phenazine center was synthesized and integrated into the graphene electrodes (Figure S12). Electrical tests conducted on the control single-molecule device, under the same conditions, consistently

https://doi.org/10.1021/jacs.4c03071
J. Am. Chem. Soc. 2024, 146, 17765−17772

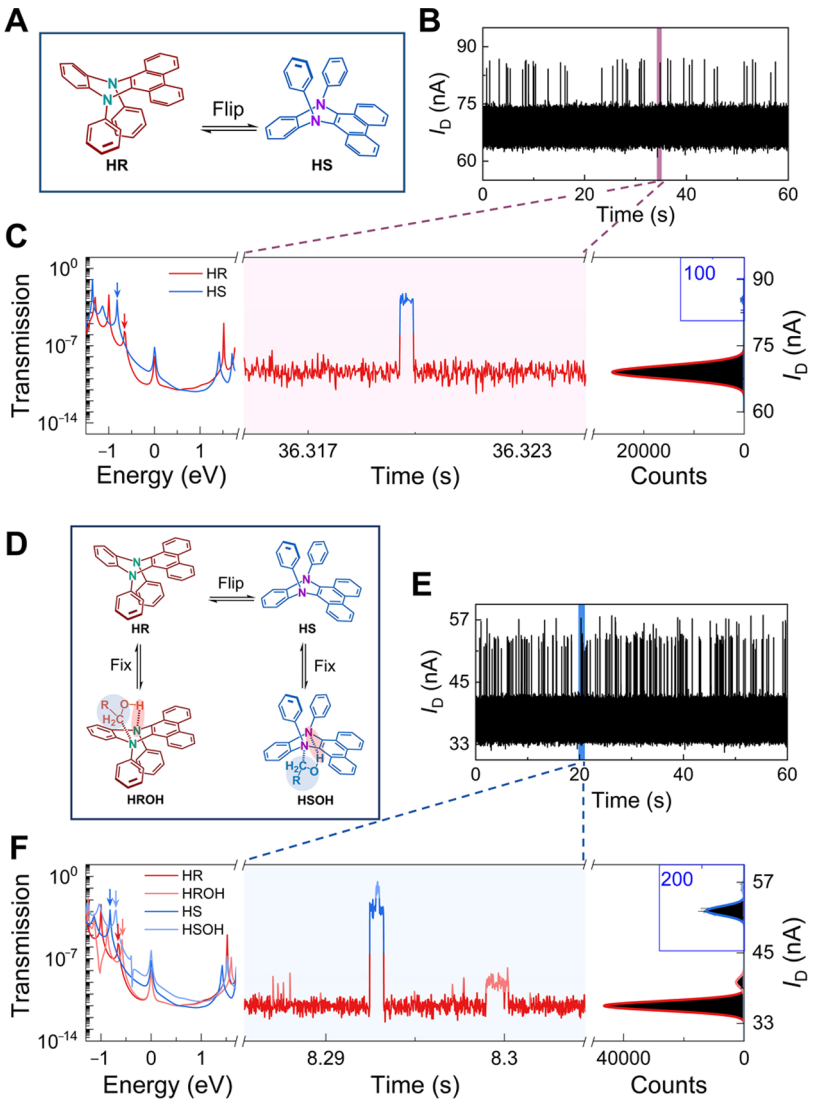

Figure 2. Proposed mechanism for the fixation process in HON-based single-molecule devices. (A) Proposed mechanism for HON-based single-molecule devices before fixation in which HR and HS denote different flipping configurations of HON. (B) Current−time (I−t) curves of HON-based single-molecule devices before fixation at 295 K with a bias voltage of 100 mV in the absence of alcohol. (C) Transmission spectra of two chiral states, enlarged I−t curves, and corresponding histogram of HON-based single-molecule devices before fixation at 295 K with a bias voltage of 100 mV; the blue inset denotes an enlarged histogram. (D) Proposed mechanism for HON-based single-molecule devices after fixation, in which HR and HS denote different flipping configurations of HON, while HROH and HSOH denote the corresponding ethanol adducts of HR and HS. (E) I−t curves of HON-based single-molecule devices after fixation at 295 K with a bias voltage of 100 mV in the presence of alcohol. (F) Transmission spectra of four chiral states, enlarged I−t curves, and corresponding histogram of HON-based single-molecule devices after fixation at 295 K with a bias voltage of 100 mV; the blue inset denotes an enlarged histogram.

exhibited the single conductance state (Figures S13 and S14), underscoring that the difference in the electrical conductance states within HON-based single-molecule devices can be predominantly attributed to the presence of the phenazine center, specifically the flexible tertiary amine center. Here, the HON molecule was connected to the single-molecule device, and the effect of input bias caused a potential drop along the molecular junction,[26] leading to the broken molecular symmetry. Thus, the stochastic switching between the electrical conductance states can be attributed to transitions between two chiral flipping states of HON (termed HR and HS) (Figure 2A). Furthermore, the transmission spectra (Figure 2C) of these two distinct chiral states were in good agreement with the conductance values in the test (Figure 2B). Although the perturbed highest occupied molecular orbital (*p*-HOMO) of HS is farther from the Fermi level of graphene in Figure 2C, it has a larger peak value, thus leading to a higher conductance. It should be mentioned that the two sides of the HON were connected to the fixed graphene electrodes through molecular engineering (due to the static device structure), which produced restricted chiral states in single-molecule junctions. The restriction magnified the influence of different chiral states on the transport structure (Figure S5), resulting in molecular chirality being effectively distinguished by conductance measurements. We also calculated the dipole moments of the molecular bridges with different chiral states used for the transmission calculation (Figure S5). The results indicated that the different chiral states caused by flipping were not completely symmetrical, which affects the transport. This is different from a previous work,[6] where the chiral center was far away from the main chain and we introduced a magnetic electrode to generate spin currents to distinguish molecules

https://doi.org/10.1021/jacs.4c03071
J. Am. Chem. Soc. 2024, 146, 17765−17772

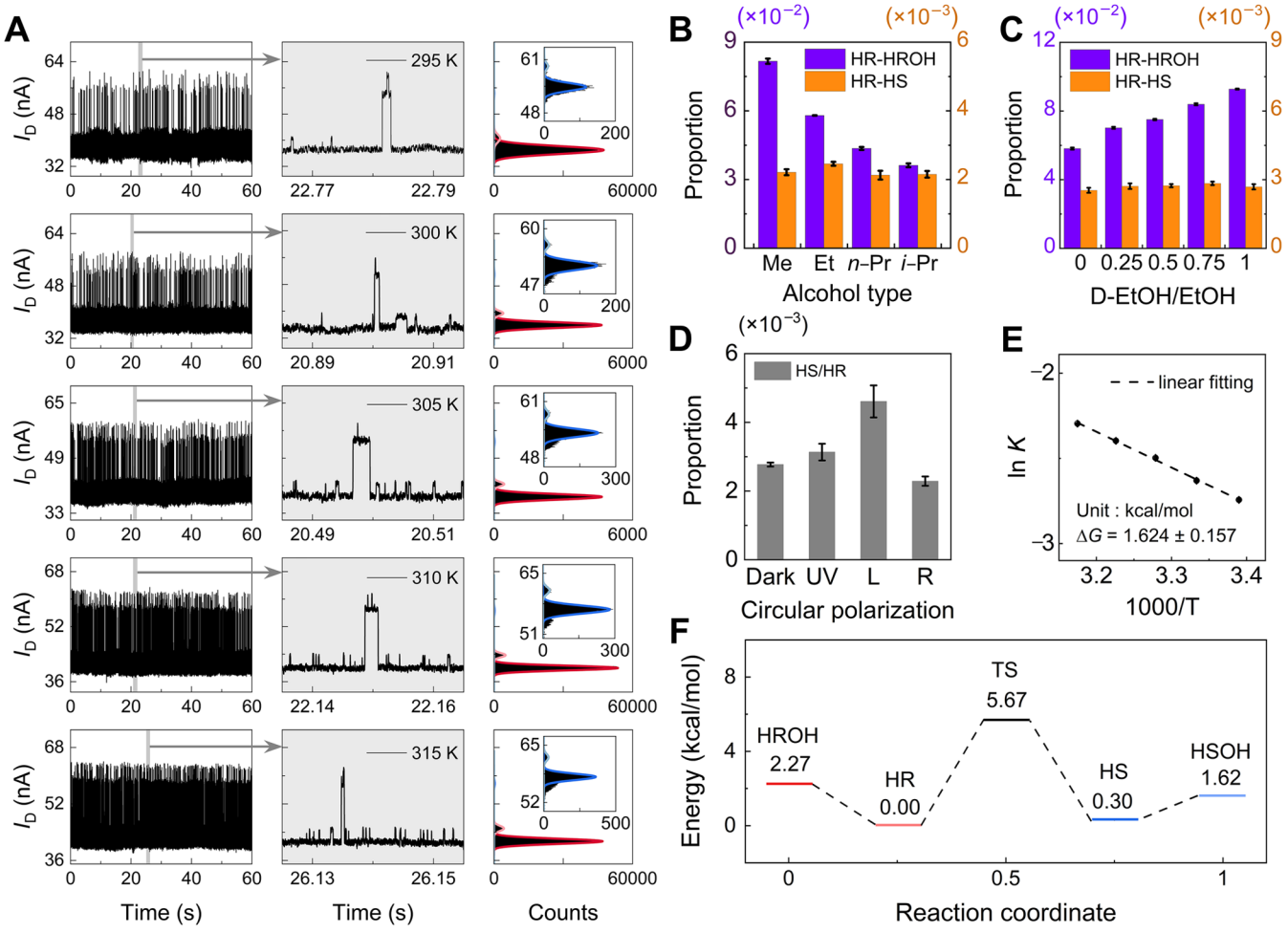

Figure 3. Mechanism validation for the fixation process in HON-based single-molecule devices. (A) *I*−*t* curves, corresponding enlarged curves, and histograms at 295, 300, 305, 310, and 315 K with an applied voltage of 100 mV, respectively. (B) Reaction degree of two processes (purple for HR to HROH and orange for HR to HS) with different types of alcohols. (C) Reaction degree of two processes (purple for HR to HROH and orange for HR to HS) with different ratios of deuterated ethanol/ethanol. (D) Regulations of different irradiation conditions (dark, nonpolarized UV, and CPLs) on the chiral transformation. R and L denote R-CPL and L-CPL, respectively. (E) Plots of the thermodynamic parameters (HR to HROH) based on the Van't Hoff equation fitting. (F) Theoretical potential energy surface calculations of the whole procedure of HON-based GMG-SMJs. Error bars in all figures were calculated from data obtained from three devices.

with different chiralities. In addition, it is observed that at lower electric fields and temperatures the low conductivity state predominates. With the increase of energy (electric field and temperature), the high conductivity state gradually appears (Figures S6−S11). This suggests that the higher conductance state represents the structure with a higher energy, which is consistent with the energy calculations of the predicted conductance states in the potential energy surface below (Figure 3F) (HS > HR). Therefore, the high and low conductance states should be ascribed to HS and HR, respectively.

Real-Time Measurement after Chirality Fixation. To explore the chirality recognition process at the single-molecule level, we needed to find a compound that could interact with the prepared chiral single-molecule device. The amination process of alcohols was chosen to construct a fixed chiral single-molecule device. To achieve this, a liquid tank filled with ethanol was added to the prepared HON single-molecule device. *I*−*V* curves before and after the addition of alcohol showed a notable increase in the conductance state types (Figures 1B and S3). Note that the addition of alcohol decreased the overall device conductance, as confirmed by control experiments using graphene transistors (Figure S15). The devices switched from their initial two-state oscillation behavior to a more complex process involving chirality fixation and recognition between four distinct conductance states (Figures 2E, 2F, and S16). Owing to the possible nucleophilic interactions between alcohols and amines, the two newly generated conductance states could potentially correspond to adducts formed by the alcohol and amine, which are renamed based on their structures as follows: HR, HROH, HS, and HSOH (Figure 2D). The transmission spectra of these four distinct states were in good accordance with the conductance values in the test (Figure 2F left). In Figure 2F, *p*-HOMOs are closer to the graphene Fermi level, which means that *p*-HOMOs dominate transport in this condition. The *p*-HOMO of HROH is more proximate to the graphene Fermi level than that of HR, and thus the conductance of HROH is higher than that of HR. Similarly, the conductance of HSOH is higher than that of HS. Although *p*-HOMOs of HS and HSOH are farther from the Fermi level of graphene than those of HR and HROH, they have larger peak values, thus leading to higher states. Therefore, the conductance of HS and HSOH is higher than that of HR and HROH. In addition, the high reversibility

https://doi.org/10.1021/jacs.4c03071
J. Am. Chem. Soc. 2024, 146, 17765−17772

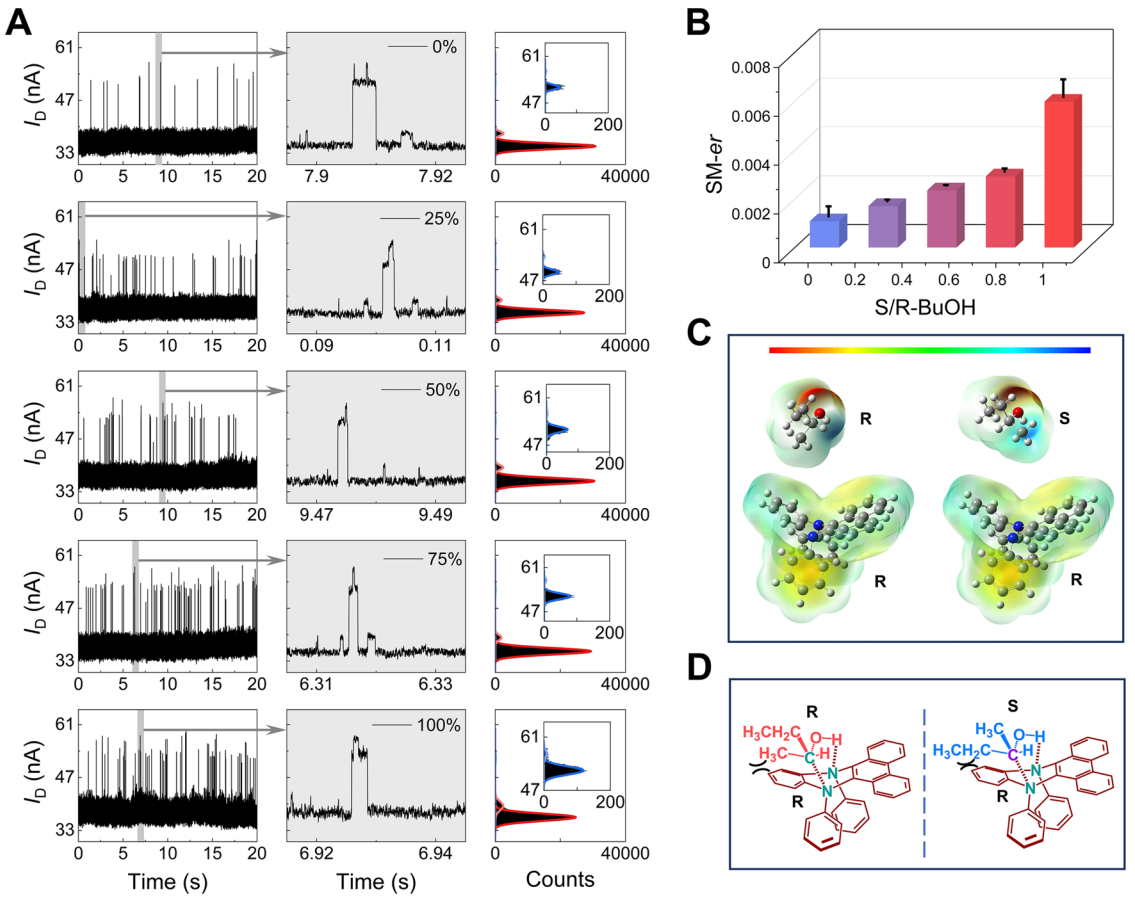

Figure 4. Chirality recognition in HON-based single-molecule devices. (A) *I*–*t* curves (T = 295 K, V = 100 mV), enlarged curves, and corresponding histograms of an HON-based single-molecule device with different ratios of S-BuOH to R-BuOH (0, 25, 50, 75, and 100%). (B) Single-molecule enantiomeric ratio (SM-*er*, HS/HR) for chirality recognition with different ratios of S-BuOH to R-BuOH. (C) Electrical effect of chirality recognition in HON-based single-molecule devices. The positive end of R-BuOH is far from the positive end of HR, indicating a low electrical repulsion. (D) Hindrance effect of chirality recognition in HON-based single-molecule devices. The hindrance between methyl and phenyl in R-BuOH and HR is less than that between ethyl and phenyl in S-BuOH and HR.

observed in the electrical tests (from HR to HROH or from HS to HSOH) can be attributed to the weak reactivity of this process, as demonstrated by macroscopic experiments.[27]

Next, temperature-dependent (Figures 3A, S17 and S18) and bias voltage-dependent experiments (Figures S19–S21) were conducted on the fixed single-molecule devices. According to the changes in conductance ratios of different molecular states with different bias voltages, the attributions of these conductance states under different bias voltages were further confirmed (Figure S22). At low bias voltages, the device predominantly displayed two conductance states: one chiral state (HR) and its corresponding ethanol adduct state (HROH). By increasing the bias voltage, another chiral state (HS) emerged, and it was accompanied by its ethanol adduct state (HSOH), ultimately leading to the emergence of all four conductance states. Furthermore, with the increase in both temperature (Figure S23) and bias voltage (Figure S24), the extent and rate of the overall reaction (amination of alcohols and chiral flipping) were progressively intensified. The thermodynamic parameter of the reaction between tertiary amines and alcohols (Figure 3E) was calculated according to previous studies,[28] and the result is in good accordance with that of the simulated potential energy surfaces (Figure 3F). The lifetime (τ) of each species was determined via single-exponential fitting of time intervals in idealized *I*–*t* curves (Figure S25) using QuB software. The determined lifetime was then employed to calculate the conversion rate constant from HR to HROH ($k = 1/\tau$). The equilibrium constant (K) of the transition from HR to HROH was determined based on the ratio of peak areas obtained from Gaussian fitting of the *I*–*t* statistical histograms at five temperatures (295, 300, 305, 310, and 315 K). The Van't Hoff equation was then used to derive the corresponding thermodynamic parameters (ΔH = 4.163 ± 0.080 kcal/mol, ΔS = 8.464 ± 0.260 cal/(mol·K), and ΔG = 1.624 ± 0.157 kcal/mol) of the HR–HROH transition.

Chirality Fixation Mechanism Verification. To further validate the proposed mechanism, a series of dependent experiments (alcohol type-dependent, isotope-dependent, and polarized light-dependent experiments) were conducted, targeting the critical sites involved in the reaction mechanism.

In this hypothesized mechanism, alcohol substituents might exert an influence on the reaction. Therefore, tests were performed using different alcohols with distinct substituents (MeOH, EtOH, *n*-PrOH, and *i*-PrOH) under uniform conditions (295 K, 0.1 V) (Figures S26–S28). The slowest reaction rate and the smallest reaction degree with HON were obtained using the alcohol with the highest steric hindrance, i.e., *i*-PrOH, whereas the highest values were obtained using the alcohol with the lowest steric hindrance, i.e., MeOH. The results of these tests indicated that alcohols with different steric

https://doi.org/10.1021/jacs.4c03071
J. Am. Chem. Soc. 2024, 146, 17765–17772

hindrances notably impact the transition from HR to HROH (Figure 3B), which unequivocally confirmed that there is some interaction between alcohols and HON molecules to some extent. With the increase in steric hindrance, the extent of reaction (HR to HROH) decreased. To clarify the possibility of hydrogen-bond interactions in the process, an isotope experiment was also conducted under uniform conditions (295 K, 0.1 V) (Figures S29−S31). In these experiments, a mixed solution of ethanol and deuterated ethanol was introduced by systematically changing the concentration of deuterated ethanol to perform the dependence test. The degree of reaction between ethanol and HON increased with the augmentation of the deuterated ethanol ratio (Figure 3C). Deuteration of ethanol in the adduct can considerably improve its stability. In addition, circularly polarized light (CPL)-dependent tests (Figure S32) were conducted on a fixed single-molecule device (Figures S33−S35). CPL can affect the chiral materials[29] and regulate the chiral reaction.[30] In these tests, a circular polarizer is used in conjunction with an ultraviolet light source (368 nm) to obtain CPL, which can excite the VIE process of HON.[23] The vibrational relaxation process occurs in excited states to obtain different vibrational ground states of HON. The HR ratio increased under right-handed CPL (R-CPL), whereas using left-handed CPL (L-CPL) increased the HS ratio (Figure 3D). At the same time, it was found that nonpolarized UV can promote the transition from HR to HS slightly. The effective CPL modulation of the transition process between chiral states (from HR to HS) proved that changes in chirality occur during this process, confirming the feasibility of the hypothesized mechanism.

Chirality Recognition on HON-based GMG-SMJs. Chirality recognition is an essential chiral phenomenon that represents the information transfer process between chiral materials, allowing a deep understanding and manipulation of chirality. Herein, the chirality recognition process between HON and added alcohol was studied. Having established that alcohols can effectively interact with HON molecules at the single-molecule level, a mixed alcohol solution comprising (R)-2-butanol (R-BuOH) and (S)-2-butanol (S-BuOH) was used to react with HON (Figures 4A, S36, and S37). Experimental results showed that alcohols with different chiralities could regulate the HON chiral properties differently (Figure 4B). HS/HR (denoted as a single-molecule enantiomeric ratio, SM-*er*) is the chirality status of a HON. For example, R-BuOH selectively promoted a HON to exhibit an R configuration and decreased SM-*er*, indicating that the interaction between R-BuOH and R-chiral HON (HR) is higher than that between R-BuOH and S-chiral HON (HS). Similarly, S-BuOH interacted more favorably with S-chiral HON (HS), inducing an increase of the S-chiral HON and uplifting SM-*er*. Thus, this phenomenon confirms the chirality recognition process between chiral alcohols and chiral tertiary amine molecules at the single-molecule level.

Based on these results and the theoretical calculations of the molecular structures, a mechanism of chirality recognition was proposed. The dipole moments of different chiral HON (HR and HS) and different chiral alcohols (R-BuOH and S-BuOH) were simulated, and their dipole−dipole interactions were separately calculated (Figure S38 and Table S1). The dipole−dipole interaction between HR and R-BuOH was approximately three times higher than that between HR and S-BuOH. The electrostatic potential diagrams, which were aligned along the reaction directions of HON and alcohol, indicated that the distance of the positive region between R-BuOH and HR is longer than that between S-BuOH and HR, and the first pair exhibited a smaller electrostatic repulsion (Figure 4C and Chapter 19 in the Supporting Information). These calculations demonstrated that molecules with identical chiralities are likely to interact with each other. Furthermore, the refined molecular structure modeling and comprehensive evaluation of spatial positional distributions proved that the binding hindrance between molecules sharing the same chirality is notably smaller. As depicted in Figure 4D, the hindrance between HR and R-BuOH was less than that between HR and S-BuOH, which can be attributed to the difference in the hindrance between the methyl or ethyl and benzene ring. These experimental phenomena and theoretical proof provide a profound understanding of the synergistic action between electrostatic interactions and steric hindrance during the intricate process of chirality recognition. This provides a deep understanding of the microscopic mechanism of chirality recognition, allowing effective use of the chirality recognition process to produce efficient chiral drugs.

CONCLUSIONS

Herein, in situ monitoring of chirality fixation and recognition on a single-molecule detection platform was successfully achieved. This real-time chirality fixation process, observed at the single-molecule level, establishes a robust experimental foundation for chirality recognition investigations. Systematic chirality recognition experiments demonstrated that chiral alcohols tend to interact with HON of the same chirality. These experimental findings and theoretical analyses clearly unveiled the intrinsic mechanism that the synergistic action between electrostatic interactions and steric hindrance occurs during the intricate chirality recognition process. The observation and mechanistic elucidation of chirality recognition at the single-molecule level enrich the understanding of this process and open a new avenue for generating chirality and synthesizing chiral compounds. Collectively, these findings contribute to a deeper understanding of chiral phenomena and provide practical prospects for the generation and utilization of chirality, driving innovation and advancement in chemistry, biology, and materials science.

ASSOCIATED CONTENT

Supporting Information

The Supporting Information is available free of charge at https://pubs.acs.org/doi/10.1021/jacs.4c03071.

Molecular synthesis for HON and control molecule, schematics of graphene transistors and single-molecule junction fabrication procedure, current−voltage curves of single-molecule junctions, statistics on single-molecule connection, theoretical analysis, electrical characterization, and the chirality recognition calculations (PDF)

AUTHOR INFORMATION

Corresponding Authors

Qi Zou − *Key Laboratory for Advanced Materials and Feringa Nobel Prize Scientist Joint Research Center, Frontiers Science Center for Materiobiology and Dynamic Chemistry, School of Chemistry and Molecular Engineering, East China University of Science and Technology, Shanghai 200237, P. R. China;* orcid.org/0000-0003-3421-9310; Email: zouqi@ecust.edu.cn

https://doi.org/10.1021/jacs.4c03071
J. Am. Chem. Soc. 2024, 146, 17765−17772

Jing-Tao Lü − *School of Physics, Institute for Quantum Science and Engineering and Wuhan National High Magnetic Field Center, Huazhong University of Science and Technology, Wuhan 430074, P. R. China;* orcid.org/0000-0001-8518-2816; Email: jtlu@hust.edu.cn

Xuefeng Guo − *Beijing National Laboratory for Molecular Sciences, National Biomedical Imaging Center, College of Chemistry and Molecular Engineering, Peking University, Beijing 100871, P. R. China; Center of Single-Molecule Sciences, Institute of Modern Optics, Frontiers Science Center for New Organic Matter, College of Electronic Information and Optical Engineering, Nankai University, Tianjin 300350, P. R. China;* orcid.org/0000-0001-5723-8528; Email: guoxf@pku.edu.cn

Authors

Weilin Hu − *Beijing National Laboratory for Molecular Sciences, National Biomedical Imaging Center, College of Chemistry and Molecular Engineering, Peking University, Beijing 100871, P. R. China*

Mingyao Li − *Beijing National Laboratory for Molecular Sciences, National Biomedical Imaging Center, College of Chemistry and Molecular Engineering, Peking University, Beijing 100871, P. R. China*

Wan Xiong − *School of Physics, Institute for Quantum Science and Engineering and Wuhan National High Magnetic Field Center, Huazhong University of Science and Technology, Wuhan 430074, P. R. China*

Shuyao Zhou − *Beijing National Laboratory for Molecular Sciences, National Biomedical Imaging Center, College of Chemistry and Molecular Engineering, Peking University, Beijing 100871, P. R. China*

He Tian − *Key Laboratory for Advanced Materials and Feringa Nobel Prize Scientist Joint Research Center, Frontiers Science Center for Materiobiology and Dynamic Chemistry, School of Chemistry and Molecular Engineering, East China University of Science and Technology, Shanghai 200237, P. R. China;* orcid.org/0000-0003-3547-7485

Complete contact information is available at: https://pubs.acs.org/10.1021/jacs.4c03071

Author Contributions

[⊥]W.H., M.L., and W.X. contributed equally to this work.

Notes

The authors declare no competing financial interest.

■ ACKNOWLEDGMENTS

We acknowledge primary financial supports from the National Key R&D Program of China (2021YFA1200101 and 2022YFE0128700), the National Natural Science Foundation of China (22150013, 21933001, 22335004, and 22175064), the New Cornerstone Science Foundation through the XPLORER PRIZE, "Frontiers Science Center for New Organic Matter" at Nankai University (63181206), and the Natural Science Foundation of Beijing (2222009).

■ REFERENCES

(1) Naaman, R.; Paltiel, Y.; Waldeck, D. H. Chiral molecules and the electron spin. *Nat. Rev. Chem.* **2019**, *3*, 250−260.

(2) Svoboda, V.; Ram, N. B.; Baykusheva, D.; Zindel, D.; Waters, M. D. J.; Spenger, B.; Ochsner, M.; Herburger, H.; Stohner, J.; Wörner, H. J. Femtosecond photoelectron circular dichroism of chemical reactions. *Sci. Adv.* **2022**, *8*, No. eabq2811.

(3) Kasprzyk-Hordern, B. Pharmacologically active compounds in the environment and their chirality. *Chem. Soc. Rev.* **2010**, *39*, 4466−4503.

(4) Le, K. V.; Takezoe, H.; Araoka, F. Chiral superstructure mesophases of achiral bent-shaped molecules−hierarchical chirality amplification and physical properties. *Adv. Mater.* **2017**, *29*, No. 1602737.

(5) Stetsovych, O.; Švec, M.; Vacek, J.; Chocholoušová, J. V.; Jančařík, A.; Rybáček, J.; Kosmider, K.; Stará, I. G.; Jelínek, P.; Starý, I. From helical to planar chirality by on-surface chemistry. *Nat. Chem.* **2017**, *9*, 213−218.

(6) Yang, C.; Li, Y.; Zhou, S.; Guo, Y.; Jia, C.; Liu, Z.; Houk, K. N.; Dubi, Y.; Guo, X. Real-time monitoring of reaction stereochemistry through single-molecule observations of chirality-induced spin selectivity. *Nat. Chem.* **2023**, *15*, 972−979.

(7) García-Vázquez, V.; Martínez-Pardo, P.; Postole, A.; Inge, A. K.; Martín-Matute, B. Synthesis of α,γ-chiral trifluoromethylated amines through the stereospecific isomerization of α-chiral allylic amines. *Org. Lett.* **2022**, *24*, 3867−3871.

(8) Moragas, T.; Liffey, R. M.; Regentová, D.; Ward, J.-P. S.; Dutton, J.; Lewis, W.; Churcher, I.; Walton, L.; Souto, J. A.; Stockman, R. A. Sigmatropic rearrangement of vinyl aziridines: Expedient synthesis of cyclic sulfoximines from chiral sulfinimines. *Angew. Chem., Int. Ed.* **2016**, *55*, 10047−10051.

(9) Grimm, J. A. A.; Zhou, H.; Properzi, R.; Leutzsch, M.; Bistoni, G.; Nienhaus, J.; List, B. Catalytic asymmetric synthesis of cannabinoids and menthol from neral. *Nature* **2023**, *615*, 634−639.

(10) Maji, R.; Ghosh, S.; Grossmann, O.; Zhang, P.; Leutzsch, M.; Tsuji, N.; List, B. A catalytic asymmetric hydrolactonization. *J. Am. Chem. Soc.* **2023**, *145*, 8788−8793.

(11) Ding, C.; Ren, Y.; Sun, C.; Long, J.; Yin, G. Regio- and stereoselective alkylboration of endocyclic olefins enabled by nickel catalysis. *J. Am. Chem. Soc.* **2021**, *143*, 20027−20034.

(12) Li, Y.; Li, Y.; Shi, H.; Wei, H.; Li, H.; Funes-Ardoiz, I.; Yin, G. Modular access to substituted cyclohexanes with kinetic stereocontrol. *Science* **2022**, *376*, 749−753.

(13) Kanj, A. B.; Bürck, J.; Vankova, N.; Li, C.; Mutruc, D.; Chandresh, A.; Hecht, S.; Heine, T.; Heinke, L. Chirality remote control in nanoporous materials by circularly polarized light. *J. Am. Chem. Soc.* **2021**, *143*, 7059−7068.

(14) Kang, J. S.; Kim, N.; Kim, T.; Seo, M.; Kim, B.-S. Circularly polarized light-driven supramolecular chirality. *Macromol. Rapid Commun.* **2022**, *43*, No. 2100649.

(15) Puriņš, M.; Waser, J. Asymmetric cyclopropanation and epoxidation via a catalytically formed chiral auxiliary. *Angew. Chem., Int. Ed.* **2022**, *61*, No. e202113925.

(16) Corey, E. J.; Ensley, H. E. Preparation of an optically active prostaglandin intermediate via asymmetric induction. *J. Am. Chem. Soc.* **1975**, *97*, 6908−6909.

(17) Evans, D. A.; Dow, R. L.; Shih, T. L.; Takacs, J. M.; Zahler, R. Total synthesis of the polyether antibiotic ionomycin. *J. Am. Chem. Soc.* **1990**, *112*, 5290−5313.

(18) Bishop, K. J. M.; Wilmer, C. E.; Soh, S.; Grzybowski, B. A. Nanoscale forces and their uses in self-assembly. *Small* **2009**, *5*, 1600−1630.

(19) Zhang, J.; Vallée, R. A. L.; Kochovski, Z.; Zhang, W.; Shen, C.; Bertram, F.; Pinna, N. Self-assembly mechanism and chiral transfer in CuO superstructures. *Angew. Chem., Int. Ed.* **2023**, *62*, No. e202305353.

(20) Yang, C.; Yang, C.; Guo, Y.; Feng, J.; Guo, X. Graphene−molecule−graphene single-molecule junctions to detect electronic reactions at the molecular scale. *Nat. Protoc.* **2023**, *18*, 1958−1978.

(21) Cao, Y.; Dong, S.; Liu, S.; He, L.; Gan, L.; Yu, X.; Steigerwald, M. L.; Wu, X.; Liu, Z.; Guo, X. Building high-throughput molecular junctions using indented graphene point contacts. *Angew. Chem., Int. Ed.* **2012**, *51*, 12228−12232.

(22) Zhang, Z.; Chen, C.-L.; Chen, Y.-A.; Wei, Y.-C.; Su, J.; Tian, H.; Chou, P.-T. Tuning the conformation and color of conjugated

polyheterocyclic skeletons by installing ortho-methyl groups. *Angew. Chem., Int. Ed.* **2018**, *57*, 9880−9884.
(23) Zhang, Z.; Song, W.; Su, J.; Tian, H. Vibration-induced emission (VIE) of N,N′-disubstituted-dihydribenzo[*a*,*c*]phenazines: fundamental understanding and emerging applications. *Adv. Funct. Mater.* **2020**, *30*, No. 1902803.
(24) Zou, Q.; Chen, X.; Zhou, Y.; Jin, X.; Zhang, Z.; Qiu, J.; Wang, R.; Hong, W.; Su, J.; Qu, D.-H.; Tian, H. Photoconductance from the bent-to-planar photocycle between ground and excited states in single-molecule junctions. *J. Am. Chem. Soc.* **2022**, *144*, 10042−10052.
(25) Yang, C.; Liu, Z.; Li, Y.; Zhou, S.; Lu, C.; Guo, Y.; Ramirez, M.; Zhang, Q.; Li, Y.; Liu, Z.; Houk, K. N.; Zhang, D.; Guo, X. Electric field−catalyzed single-molecule Diels-Alder reaction dynamics. *Sci. Adv.* **2021**, *7*, No. eabf0689.
(26) Lang, N. D.; Avouris, P. Understanding the variation of the electrostatic potential along a biased molecular wire. *Nano Lett.* **2003**, *3*, 737−740.
(27) Liu, Z.; Yang, Z.; Yu, X.; Zhang, H.; Yu, B.; Zhao, Y.; Liu, Z. Efficient cobalt-catalyzed methylation of amines using methanol. *Adv. Synth. Catal.* **2017**, *359*, 4278−4283.
(28) Yang, C.; Zhang, L.; Li, H.; Guo, Y.; Jia, C.; Zhu, W.; Mo, F.; Guo, X. Single-molecule electrical spectroscopy of organocatalysis. *Matter* **2021**, *4*, 2874−2885.
(29) Ma, Q.; Chen, L.; Xia, F. Chiral nanofluidic membrane for detection of circular polarization light. *Matter* **2022**, *5*, 1345−1347.
(30) Hao, C.; Wang, G.; Chen, C.; Xu, J.; Xu, C.; Kuang, H.; Xu, L. Circularly polarized light-enabled chiral nanomaterials: From fabrication to application. *Nano-Micro Lett.* **2023**, *15*, No. 39.

https://doi.org/10.1021/jacs.4c03071
J. Am. Chem. Soc. 2024, 146, 17765−17772